Monthly Notices
of the
ROYAL ASTRONOMICAL SOCIETY

MNRAS **480,** 751–758 (2018)
Advance Access publication 2018 July 07

doi:10.1093/mnras/sty1801

Breaking the spectral degeneracies in black hole binaries with fast timing data: the hard state of Cygnus X-1

Magnus Axelsson[1,2]★ and Chris Done[3]

[1]*Oskar Klein Center for CosmoParticle Physics, Department of Physics, Stockholm University, SE-106 91 Stockholm, Sweden*
[2]*Department of Astronomy, Stockholm University, SE-106 91 Stockholm, Sweden*
[3]*Department of Physics, Durham University, South Road, Durham DH1 3LE, UK*

Accepted 2018 July 3. Received 2018 June 27; in original form 2018 March 2

ABSTRACT

The spectra of black hole binaries in the low/hard state are complex, with evidence for multiple different Comptonization regions contributing to the hard X-rays in addition to a cool disc component. We show this explicitly for some of the best *RXTE* data from Cyg X-1, where the spectrum strongly requires (at least) two different Comptonization components in order to fit the continuum above 3 keV, where the disc does not contribute. However, it is difficult to constrain the physical properties of these Comptonization components uniquely using spectral data alone. Instead, we show that additional information from fast variability can break this degeneracy. Specifically, we use the observed variability power spectra in each energy channel to reconstruct the energy spectra of the variability on time-scales of ∼10, 1, and 0.1 s. The two longer time-scale spectra have similar shapes, but the fastest component is dramatically harder, and has strong curvature indicating that its seed photons are not from the cool disc. We interpret this in the context of propagating fluctuations through a hot flow, where the outer regions are cooler and optically thick, so that they shield the inner region from the disc. The seed photons for the hot inner region are then from the cooler Comptonization region rather than the disc itself.

Key words: accretion, accretion discs – X-rays: binaries – X-rays: individual: Cygnus X-1.

1 INTRODUCTION

The energy spectra of the low/hard state of black hole binaries have complex curvature, and robustly require additional components as well as the well-known 'disc plus power law'. This is shown most clearly in spectra spanning the broadest bandpass (Makishima et al. 2008; Nowak et al. 2011), but even in 3–100 keV data alone (e.g. from *RXTE*) the continuum shape has a clear hardening beyond 10 keV, which cannot be accounted for by reflection alone (unless the reflection parameters are extreme: Fabian et al. 2014). Nowak et al. (2011) show that this can be modelled by several different continuum components, which could plausibly derive from a radial stratification of temperature and/or optical depth of the Comptonizing hot flow (Di Salvo et al. 2001; Ibragimov et al. 2005; Makishima et al. 2008; Yamada et al. 2013; Basak et al. 2017). Alternatively, this curvature could arise from a completely different region, potentially indicating synchrotron emission from the jet (Markoff, Nowak & Wilms 2005). Conversely, the curved spectrum could arise from a single region if the electron distribution is not completely thermal (hybrid thermal/non-thermal models: Poutanen & Coppi 1998; Gierliński et al. 1999; Ibragimov et al. 2005). Plainly, spectral fitting alone is highly degenerate, but the longer term spectral evolution in the low/hard state, where the overall spectrum softens with increasing luminosity, can be generally interpreted in models where the inner disc evaporates into a hot flow above the innermost stable circular orbit. Decreasing this truncation radius with increasing mass accretion rate leads to stronger disc emission, which leads to stronger Compton cooling and a softer spectrum, as observed (see, e.g. the review by Done, Gierliński & Kubota 2007). Multiple Comptonization regimes are quite naturally expected in this geometry as the part of the hot flow closest to the truncated disc is more strongly illuminated, so should have a softer spectrum than the inner parts of the hot flow closest to the black hole.

Here, we use the additional information from spectral evolution during fast variability in the low/hard state to determine the continuum component shapes, and hence better constrain their physical origin. The fast variability (time-scales of order 10 s to a few tens of milliseconds) can plausibly be stirred up at all radii, but then propagates through the accretion flow towards the black hole (Lyubarskii 1997; Kotov, Churazov & Gilfanov 2001; Arévalo & Uttley 2006). Propagation is governed by the local viscous time-scale, which strongly damps any faster variability. The local viscous time is a function of radius, so the inner regions of the flow can generate

★ E-mail: magnusa@astro.su.se

faster fluctuations than the outer radii, coupling time-scale and radii together. If the hot flow is also *spectrally* stratified with radius, then this couples time-scale and spectrum together as well. This can quantitatively explain the otherwise very puzzling observation that fluctuations in the light curves of a hard and soft band are highly correlated, but with the hard lagging behind the soft on a time-scale which varies with the variability time-scale (Kotov et al. 2001).

Several studies have looked at the energy spectrum of specific features in the power spectrum (such as quasi-periodic oscillations) in BHB sources, but analyses of the broad-band variability are much less frequent. The technique was pioneered by Revnivtsev, Gilfanov & Churazov (1999), who looked at the energy spectra of Cyg X-1 in three different frequency ranges. However, the focus of their study was to the iron line features, whereas we use this to isolate the spectral shapes of the broad band continuum components associated with different frequencies of variability in the low/hard state of Cyg X-1.

We summarize the data and analysis technique in Section 2 and present our results in Section 3. Finally, we discuss our findings in Section 4.

2 DATA ANALYSIS

Cygnus X-1 is perhaps the most studied of all black hole binaries, with over 1000 observations using the *RXTE* satellite alone. Its variability has been extensively reported in a number of studies, spanning time-scales from milliseconds to years (e.g. Revnivtsev, Gilfanov & Churazov 2000; Reig, Papadakis & Kylafis 2002; Zdziarski et al. 2002). Here, we focus on the broad-band variability in the 0.05–30 Hz range seen in the hard spectral state. The fractional rms in this state is ∼30 per cent, and the power spectrum is well described by a combination of two or more Lorentzian components. The peak frequency of these components vary on both long and short time-scales, and are correlated with spectral changes (e.g. Nowak 2000; Pottschmidt et al. 2003; Axelsson, Borgonovo & Larsson 2005).

The study is performed using archival data of Cygnus X-1 from the Proportional Counter Array (PCA; Jahoda et al. 1996) instrument onboard the *RXTE* satellite, covering the energy range 3–35 keV. Due to an antenna failure early on in the mission, most observations were performed using data modes where spectral resolution is lower to achieve high temporal resolution. To maximize the power of the analysis, we searched for all observations where the data mode B_16ms_64M_0_249 is available (a total of eight ObsIDs), giving a good balance between spectral and temporal resolution. This mode allows us to extract 39 channels in the energy range 3–30 keV with a time resolution of 16 ms, giving an upper limit of ∼30 Hz for the power spectra. The lower range was chosen to be 0.01 Hz. In the spectral fit, we also include data from the HEXTE instrument for the total spectrum, covering the energy range from 40 to 200 keV.

All observations in the selected data mode are taken in the low/hard state, with only small differences in luminosity and spectral shape. We choose the longest observation as this has the best signal-to-noise ratio, taken on 1996-03-30 (MJD 50172; ObsID 10238-01-05-000, 13 ks exposure). These data have been used in many previous studies, including the frequency-resolved analysis of Revnivtsev & Gilfanov (2006).

The PCA data were extracted using the standard *RXTE* tools of `HEASoft` version 6.21, combining data from all five PCUs and applying standard screening criteria: elevation $>10^{\circ}$, offset <0.02 and a 30-min exclusion after each SAA passage. Background spectra

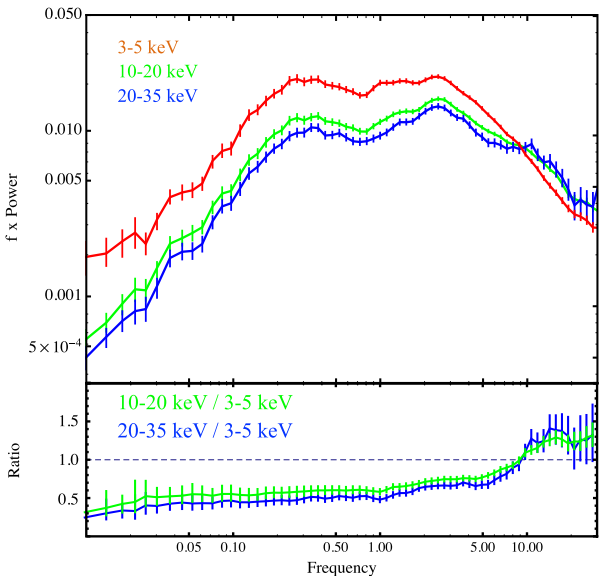

Figure 1. Upper panel: power spectra in three energy bands from ObsID 10238-01-05-000: 3–5 keV (red), 10–20 keV (green), and 20–35 keV (blue). Lower panel: ratio of power of the 10–20 keV band (green) and 20–35 keV band (blue) compared to the 3–5 keV band.

were extracted from data files generated by the tool `pcabackest` and the latest background model for bright sources (released Aug 6, 2006). Finally, response matrices were generated using the `pcarsp` script. A systematic error of 1 per cent was added to the spectra.

For the HEXTE spectrum, data were extracted from Cluster A. As in the case of the PCA data, we followed the standard procedure described in the *RXTE* cookbook[1] to produce source and background spectra.

Power density spectra were produced from the PCA light curves in 130 s intervals. These individual power spectra were then averaged, and deadtime correction applied and the Poissonian noise level subtracted (Zhang et al. 1995). We used the normalization of Leahy et al. (1983), converted into squared fractional rms (Belloni & Hasinger 1990; Miyamoto et al. 1991). To make the frequency-resolved spectra, we followed the same technique as in Axelsson, Hjalmarsdotter & Done (2013). We extracted the light curve for every available energy channel and constructed its power spectrum, which was then fit with three Lorentzian components (see, for example, Belloni, Psaltis & van der Klis 2002). We used the parametrization of Axelsson et al. (2005), meaning that the frequencies reported correspond to the peak of the Lorentzian component in the frequency×power versus frequency representation.

3 RESULTS

3.1 Power spectra

In the first step of the analysis, we extract the power spectrum in three broad energy ranges to get a view of its overall evolution with energy. The bands used for this were 3–5 keV (red/top), 10–20 keV(green/middle), and 20–35 keV (blue/bottom) in Fig. 1. There are two distinct features in the power spectrum, with excess of

[1] http://heasarc.gsfc.nasa.gov/doc/xte/recipes/hexte.html

Table 1. Peak frequencies (in the frequency×power versus frequency representation) of the three Lorentzian components in the three broad energy bands.

	ν_1 (Hz)	ν_2 (Hz)	ν_3 (Hz)
3–5 keV	0.29 ± 0.01	2.3 ± 0.1	–
10–20 keV	0.30 ± 0.01	2.3 ± 0.1	9.3 ± 1.3
20–35 keV	0.32 ± 0.02	2.3 ± 0.1	9.3 ± 0.9

power around 0.2 and 2 Hz. The overall shape of the power spectrum is similar between the bands, except that the lowest energies have higher normalization (and hence higher total rms power) except at the very highest frequencies. This can be seen more clearly in the lower panel of Fig. 1, which shows the ratio of the power spectra in the mid and high energy bands to that at low energies. The ratio switches from being fairly constant at low frequencies (less than 3 Hz), but then rising sharply to a much higher ratio above 10 Hz. This shows that there is a third feature in the power spectrum at high frequencies, but that this has a marked energy dependence, being much stronger at higher energies. Such a feature (and also a fourth component at even higher frequencies) has been reported in previous studies (e.g. Pottschmidt et al. 2003).

We fit the three power spectra using three Lorentzian functions and study the peak frequency in each band. The results are presented in Table 1. We find that the frequencies do not show any significant energy dependence.

3.2 Time-averaged spectrum

We first attempt to fit the time-averaged spectrum, using both PCA and HEXTE data, with a single Comptonization region, similar to the fits in Axelsson et al. (2013). This consists of thermal Comptonization, parametrized using the model NTHCOMP (Zdziarski, Johnson & Magdziarz 1996; Życki, Done & Smith 1999) in XSPEC. We also include reflection (XILCONV; Kolehmainen, Done & Díaz Trigo 2011; García et al. 2013) and relativistic smearing (KDBLUR; Laor 1991; Fabian et al. 2002) of the Comptonized emission. For the smearing, the outer radius was left frozen at the default value of 400 r_g whereas the inner radius ($r_{\rm in}$) was left free. We characterize the interstellar absorption using use TBNEW_GAS, the updated version of TBABS (Wilms, Allen & McCray 2000), with the assumption that all absorbing matter is neutral gas. The column density was frozen to $0.6 \times 10^{22}\,{\rm cm}^{-2}$ (a typical hard state value; see, e.g. Nowak et al. 2011; Miškovičová et al. 2016). We also include a normalization constant between HEXTE and PCA. This was initially left free, but we found that the value did not change between models, always staying consistent with 0.9. It was therefore frozen to this value. We do not include a thermal component from the disc as the data cover energies only above 3 keV, which is too high to include much emission from a typical low/hard state temperature of 0.2 keV (Ibragimov et al. 2005). At first the input seed photon temperature to our Comptonization component is left free in the range of 0.1–0.5keV. Values lower than ∼0.3 keV are statistically favoured, with a χ^2 minimum close to 0.2 keV; however, all values below the limit are acceptable. The other parameter values stay compatible within errors, and we therefore choose to freeze the seed photon temperature at 0.2 keV.

Our single-Comptonization model is unable to provide a good fit to the data. Even the very first attempt, where all parameters were left free, gives a reduced χ^2 of 145/97, well above unity. Furthermore, this value is only found when the column density approaches zero, which is not a plausible result. Putting a conservative lower limit requiring the column density to be $>0.4 \times 10^{22}\,{\rm cm}^{-2}$ raises the χ^2-value to 180.

The poor χ^2-value from our model is in itself not enough to immediately rule out a single-Comptonization scenario, as there are many other potential variations, and more powerful instruments than *RXTE* for spectral studies. However, it does show that these data follow the same pattern as seen in previous studies (e.g. Ibragimov et al. 2005; Makishima et al. 2008; Nowak et al. 2011; Hjalmarsdotter, Axelsson & Done 2016), and are in that sense representative of black hole binaries in the hard state. Taken together with the many results pointing to inhomogeneous Comptonization being present in Cyg X-1 (see Section 1), it is clear there is more complexity in the data than our first model can accommodate.

Following Ibragimov et al. (2005), we therefore add a second thermal Comptonization component, again with seed photon temperature frozen to 0.2 keV. In terms of XSPEC components, the model becomes TBNEW_GAS×(NTHCOMP+NTHCOMP+KDBLUR×XILCONV ×(NTHCOMP+NTHCOMP)). Note that XILCONV is set to output only the reflected emission, and the parameters of its NTHCOMP arguments are tied to those of the direct emission. This now gives an excellent fit to the data (a nested model F-test gives a chance probability $\ll 10^{-20}$, indicating a highly significant improvement). Details of the fit are given in Table 2, along with the single Comptonization model for comparison.

The reduced χ^2 value for our two-component fit is well below 1; this is due to the 1 per cent systematics added to the data, which dominates over the statistical uncertainty. Including a simple 1 per cent systematics gives a conservative upper limit on the response uncertainties. With 1 per cent systematics, $\chi^2/{\rm dof} \gg 1$ (as for the single-Comptonisation model) means that the fit is unacceptable at high confidence even given response uncertainties. However, the conservative approach results in $\chi^2/{\rm dof} \ll 1$ when an additional component is added. We chose this approach as the point is simply to show that the spectra require something more complex than a single Comptonization component and its reflection.

We stress that while the two-component fit found here is the best fit using this model, it is not necessarily comparable to those found in other studies, and it is not unique. Indeed, previous analyses have found that a wide range of combinations of two Comptonization regions are able to provide good fits to the spectrum of Cyg X-1. Depending on the exact data set used, and using assumptions such as setting the same electron temperature for both regions, varying non-thermal electron fractions and different variations of the Comptonization model, different conclusions are drawn about the properties of the Comptonisation (see, e.g. Ibragimov et al. 2005; Makishima et al. 2008; Nowak et al. 2011; Mahmoud & Done 2018a). This divergent set of results underscores the degeneracy inherent in spectral analysis, stressing the need also to consider information from temporal analysis.

3.3 Frequency resolved spectra

In the next step, we extracted the frequency-resolved spectrum. We found that allowing the peak frequencies of the three Lorentzian components (L_1, L_2 and L_3) to vary in every channel led to very large uncertainties, and therefore froze the peak frequencies to the average of those found in Table 1: 0.3, 2.3, and 9.3 Hz. This is justified since the frequencies did not change significantly between the energy bands (Table 1). With this approach we were able to constrain the components up to ∼30 keV, above which the signal became too weak. In the first few channels, the highest frequency

Table 2. Parameter values for the best fit of the total spectrum to the spectral model using one or two thermal Comptonization components. Subscripts s (soft) and h (hard) denote the two Comptonization components, both of which have seed photons set to a 0.2 keV blackbody.

Model	kT_s (keV)	Γ_s	$norm_s$	kT_h (keV)	Γ_h	$norm_h$	R	$\log \xi$	r_{in} (r_g)	χ^2/dof
One Comp.	–	–	–	480^{+600}_{-160}	$1.68^{+0.002}_{-0.002}$	$1.86^{+0.04}_{-0.04}$	$0.37^{+0.03}_{-0.03}$	$3.30^{+0.01}_{-0.01}$	45^{+unc}_{-20}	216.9/100
Two Comp.	$1.8^{+0.3}_{-0.3}$	$2.01^{+0.23}_{-0.10}$	$0.56^{+0.08}_{-0.21}$	116^{+20}_{-14}	$1.66^{+0.02}_{-0.01}$	$1.94^{+0.09}_{-0.10}$	$0.27^{+0.04}_{-0.04}$	$2.98^{+0.08}_{-0.12}$	7^{+5}_{-2}	52.2/97

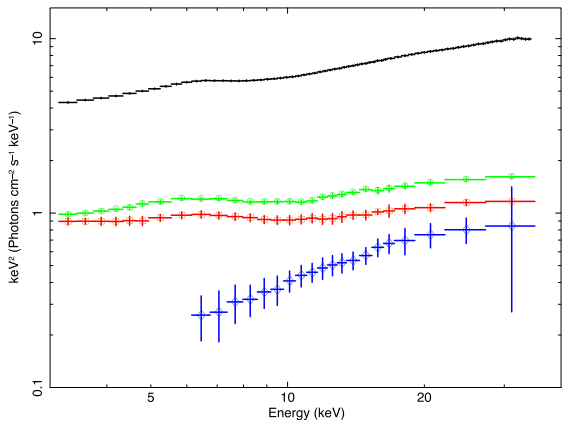

Figure 2. Upper panel: extracted spectra from the three components in the power spectrum. In order of rising peak frequency: red squares (L_1), green circles (L_2), and blue diamonds (L_3). The total spectrum (black) is also shown for comparison. While L_1 and L_2 show spectra similar to the total, L_3 is dramatically different.

component is very weak, and its normalization is consistent with being zero. We integrate each Lorentzian in each energy channel to get an rms for that component at that energy, and multiply the time-averaged count rate by this value to extract frequency-resolved spectra corresponding to the noise components L_1 (red squares), L_2 (green circles), and L_3 (blue diamonds). These are presented along with the total spectrum in Fig. 2, where all the data are shown deconvolved against a power law of index −2 (i.e. flat in the νF_ν representation) to aid in the comparison.

L_1 and L_2 (red squares and green circles) show similar appearance to each other and to the total spectrum below 10 keV, including features around the 6.4 keV iron line, indicating reflection. However, both are much softer than the total spectrum above 10 keV. This is consistent with the study using *AstroSat* data presented by Misra et al. (2017), who found that the lower frequency component weakens more at higher energies. We see the same trend in our data (Fig. 2).

The most surprising behaviour is seen in the highest frequency component, L_3. As expected, it is not detected at low energies, likely being too weak. However, at higher energies the spectrum is radically different from the other two, more resembling a single power law than the total spectrum. It is also significantly harder and has no obvious reflection features (see also Revnivtsev et al. 1999).

The data from the variability components were then individually fit, using the spectral model from the total spectrum as template. The model was changed in steps until an acceptable fit was found. In the first step, the best-fitting model for the total spectrum was merely scaled down, and tested against the data. Not surprisingly, this did not fit any of the variability components. L_1 and L_2 are softer than the total spectrum, whereas L_3 is too hard. In the second step, the relative normalization between the two Comptonization components was allowed to vary. This allowed us to find acceptable fits for L_1 and L_2, but not for L_3.

As L_3 is much harder than the total spectrum, it is clear that the slope of the hard Comptonization component must change to provide a good fit. We therefore allowed this parameter to vary. However, we were still not able to find a good fit, unless we also let the seed photon temperature increase. Together, these two changes allowed us to find an acceptable fit to L_3 using a single Comptonization component; no reflection is required. It seems then that L_3 provides us with a 'pure' description of the hard Comptonization.

In order to utilise this information, we now refit the total spectrum and L_3 together, tying the hard Comptonization in the total spectrum to the variability spectrum, and allowing for different seed photon temperatures in the two Comptonization components. The resulting fit quality is comparable to the one found before, but with the advantage that also L_3 can be fit. As before, allowing the relative normalization to vary also allows good fits to L_1 and L_2. The results are presented in Table 3, and the resulting spectra with residuals shown in Fig. 3.

We note that the electron temperature of the soft Comptonization component is almost comparable to the seed photon temperature of the hard Comptonization. Attempting to tie these parameters gives an acceptable fit, yet slightly worse compared to those presented in Table 2. We therefore leave them separated.

The parameters in Table 3 also allow us to look at the ratio between normalization parameters for the soft and hard Comptonization components. This ratio ($norm_s/norm_h$) is 268 for L_1 and 216 for L_2, making it clear that the hard Comptonization is relatively stronger in L_2 than in L_1. The same ratio is 112 in the total spectrum, indicating that the hard Comptonization is less pronounced in the variability spectra compared to the total spectrum.

Finally, we compare the best-fitting model found using the variability components with that presented in Table 2. The main difference between the models is that the seed photon temperature of the hard Comptonization component is no longer set to 0.2 keV. Instead, we fix it at 3 keV, as indicated by the spectrum of L_3. Surprisingly, the resulting fit proves to be a significant improvement over the result in Table 2, with a χ^2 of 34.7 compared to 52.2. Fig. 4 shows a direct comparison between the two fits. Although both models give a good fit, using a higher seed photon temperature gives a significantly better fit statistic, and the PCA residuals improve. The model found by considering also the temporal information has thereby led to a better global fit, and Monte Carlo simulations show that the chance probability of such an improvement is $<3 \times 10^{-5}$, assuming the lower temperature is the correct model. This further strengthens the result that the two Comptonization regions are spatially distinct, with the harder region seeing much more energetic seed photons.

The high seed photon temperature required by the data implies that the innermost region (where L_3 arises) is shielded from the disc photons. This, in turn, suggests that Comptonized emission arising in this region would not reach the disc, and thereby not be reprocessed. Unfortunately, the spectrum of L_3 does not allow us to test this prediction, as the uncertainties on the data are large (cf. the direct emission and reflection in Fig. 4B). Allowing only the low-temperature Comptonization component to be reflected in the total spectrum gives an acceptable but worse fit compared to the one

Table 3. Parameter values for the best fit to the spectral model TBNEW_GAS×(NTHCOMP+NTHCOMP+KDBLUR ×XILCONV ×(NTHCOMP+NTHCOMP)). The total spectrum and the three variability components were all fit together. Subscripts s (soft) and h (hard) denote the two Comptonization components.

Comp	$kT_{e,s}$ (keV)	Γ_s	$norm_s$	$kT_{seed,h}$ (keV)	$kT_{e,h}$ (keV)	Γ_h	$norm_h$ (10^{-2})	R	$\log\xi$	r_{in} (r_g)	χ^2/dof
Total	$2.1^{+0.2}_{-0.2}$	$1.93^{+0.03}_{-0.03}$	$2.82^{+0.11}_{-0.48}$	3.1†	145^{+50}_{-32}	$1.69^{+0.02}_{-0.03}$	$1.8^{+0.4}_{-0.6}$	$0.24^{+0.10}_{-0.05}$	$3.00^{+0.24}_{-0.19}$	$5.1^{+2.3}_{-1.5}$	61.6/171
L_1	”	”	$0.59^{+0.02}_{-0.02}$	”	”	”	$0.22^{+0.01}_{-0.01}$	”	”	”	
L_2	”	”	$0.67^{+0.01}_{-0.01}$	”	”	”	$0.31^{+0.01}_{-0.01}$	”	”	”	
L_3	–	–	–	$3.1^{+0.5}_{-0.3}$	”	”	$0.20^{+0.03}_{-0.03}$	–	–	”	

†Value tied to that from L_3.

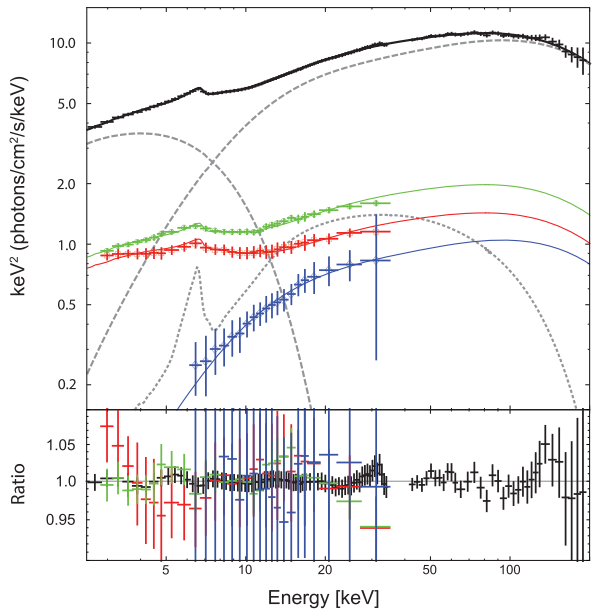

Figure 3. Fits of the total spectrum (black points) and frequency-resolved spectra (red squares, green circles and blue diamonds). The gray lines show the Comptonization (dashed) and reflection (dotted) components in the total spectrum. Solid lines show the total spectrum for both the total spectrum as well as each individual frequency-resolved spectrum. The bottom panel shows the ratio between the data and fitted model.

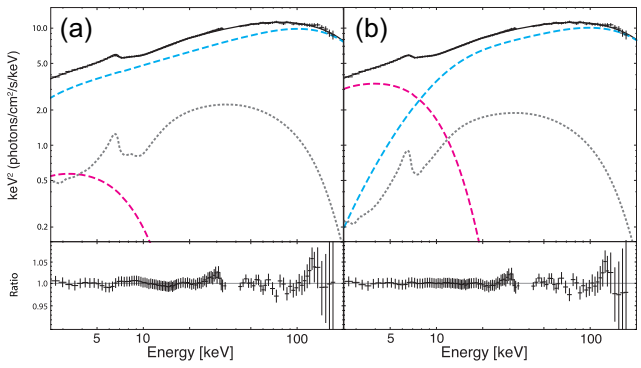

Figure 4. Comparison of spectral fits using different seed photon temperature for the hard Comptonization component. A: Original model using $kT_{seed,h} = 0.2$ keV. χ^2/dof = 52.2/97. B: Model using $kT_{seed,h} = 3$ keV, as indicated by the variability spectra. χ^2/dof = 34.7/97. Upper panels show the data and model components: soft Comptonization (dashed magenta/dark grey), hard Comptonization (dashed cyan/light grey) and reflection (dotted line). Lower panels show the ratio between data and model.

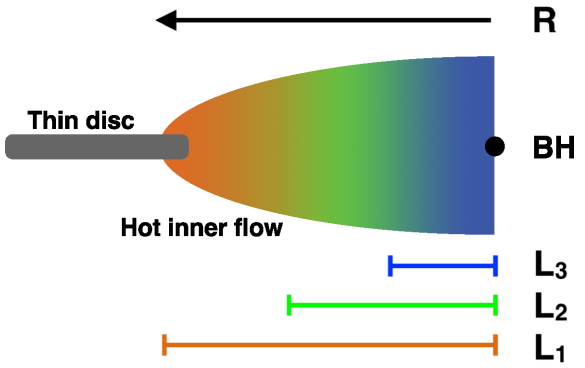

Figure 5. Cartoon picture showing the disc (grey) and regions of the inner accretion flow contributing to each variability component.

in Table 3 (χ^2/dof of 74.3/171 compared to 61.1/171). We therefore choose to keep the fit where both Comptonization components are reflected. However, the worsening of the fit when considering the shielding effect of the softer component could be an indication that there are details in the data which our two-component model is unable to capture. We try to constrain these additional features in a model independent way below.

3.4 Isolating different radii

As described in Section 1, the broad-band variability likely arises due to propagating fluctuations in the accretion flow. In this picture, slower fluctuations arise in the outer regions of the flow, and as they propagate inwards, more rapid fluctuations are added. Variability at a given frequency is produced at a characteristic radius, so includes the spectrum produced at that radius, but then it propagates inwards so it is the sum of different spectral components at all radii interior to that where the characteristic frequency of the component is generated. This is shown schematically shown in Fig. 5, where the sketch is of a gradually stratified flow, with each region contributing a harder spectrum as the radius decreases, rather than the two component model used above. A fundamental assumption of this picture is that smaller radii correspond to harder spectra. We will discuss this in Section 4.

The cartoon image of Fig. 5 reveals a model-independent way to extract the spectra as a function of radius. By studying the *difference* between the variability spectra, we can attempt to isolate the spectrum which is characteristic of the radius at which each variability component is produced.

As described above, the highest frequencies are expected to be the ‘cleanest’, i.e. only present in the innermost region and thereby modulating the emission from the fewest emission components. This is supported by our result that the spectrum of L_3 is well-fit by a single pure Comptonization component. L_2 has a lower frequency,

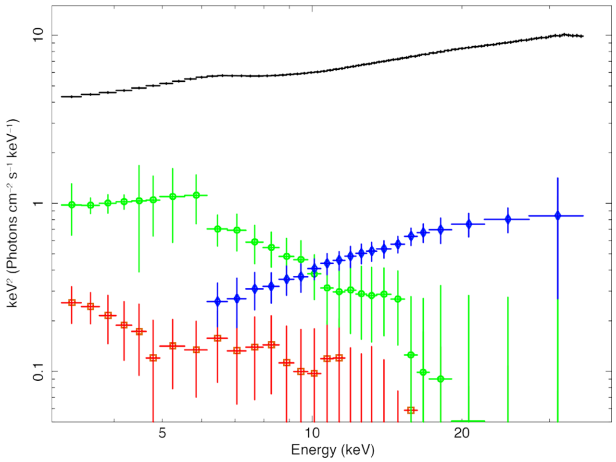

Figure 6. Spectra of each variability component after subtracting the contribution from higher frequencies (smaller radii). Colours and symbols are the same as in Fig. 2.

and it should therefore contain the same contributions as L_3, as well as emission from larger radii. To isolate the emission in the regions successively further out, we rescaled the L_3 spectrum to match that from L_2 in the highest energy bin (where the contribution is dominated by the innermost region), and then subtracted the L_3 spectrum. This is the maximum contribution from the hard innermost region, so this spectrum is the softest that can be characteristic of the region where L_2 is produced. Similarly, we rescaled and subtracted the spectrum of L_2 from L_1. The results are shown in Fig. 6.

While the data points have large uncertainties, some general features can still be distinguished. The spectrum characteristic of the largest radii (red squares) is the softest, and is subtly different to the shape of the soft Comptonization in our two-component fits. The spectrum which can be associated with L_2 (green circles) is appreciably harder than that of L_1, while that of L_3 is well described by a single hard Comptonization component with high electron temperature and seed photons around a few keV (as above).

These results suggest a more complex flow than in our two component model fits, hinting that the spectrum should be modelled allowing for an even greater number of emission regions. Unfortunately, the data do not allow us to explore this further. However, it is clear that the technique has the potential to reveal even greater details of the stratified flow than shown in this study when combined with new data from *NICER* and/or *AstroSat*.

4 DISCUSSION

It has been known for a long time that there are more than two components in the broad-band variability spectrum of Cyg X-1 (e.g. Nowak 2000; Pottschmidt et al. 2003). However, the frequency range studied here (0.01–30 Hz) is dominated by two components, with a third entering only in the hardest observations (Axelsson et al. 2008). It is therefore interesting to see the presence of this third component in the higher energy bands, even when it is not evident in the lowest band.

Previous results have shown that the variability components change in response to spectral evolution of the source, becoming weaker and moving to higher frequencies as the hardness decreases (Pottschmidt et al. 2003; Axelsson et al. 2005; Axelsson, Borgonovo & Larsson 2006; Grinberg et al. 2014). Our results indicate that there is also an energy dependence present. Because the frequencies do not change between the energy bands, it is likely that the third variability component appears due to increased relative strength as the energy increases – this is additionally supported by its hard spectrum. Having the strength of the component vary with energy also explains the result of Nowak (2000), who found that the best–fitting combination of Lorentzian functions matching the power spectrum was dependent on energy.

Our data show the same complexity as seen in most hard state observations of Cyg X-1. Indeed, this is a general feature in many BHB systems (e.g. Ibragimov et al. 2005; Makishima et al. 2008; Yamada et al. 2013; Hjalmarsdotter et al. 2016), and many authors have concluded that multiple Comptonization regions are needed. This result is further strengthened by the addition of the frequency-resolved data. While it is clear that both L_1 and L_2 show signs of Comptonization, they are both softer than the total spectrum. It is thus not possible for a single Comptonization spectrum to explain both their spectra and the total. The point is further underscored by L_3, which appears to match a clean Comptonization spectrum, yet this spectrum is much too hard to explain the softer spectra. The only alternative is to allow multiple Comptonization regions.

If there are indeed two (or more) separate Comptonization components, as suggested by both the spectrum and the variability, they cannot be completely independent. If the two components would vary randomly with respect to each other, the rms is expected to be lower in the energy range where they contribute equally, as opposed to where one component dominates. There is no indication of such behaviour, either in the observations studied here or in previous works (e.g. Revnivstev, Gilfanov & Churazov 2001).

The smooth evolution of the rms instead supports the view of variability propagating through the flow, with each radius contributing most strongly at frequencies close to the local viscous time-scale. Slower variations from the outer regions then modulate the faster variability, naturally coupling the variability at different time-scales. This picture also couples higher frequencies to regions closer to the black hole, predicting that the energy spectrum of the variability components will get harder with increasing frequency. This matches the observations reported here, as well as many previous results.

While the slight differences between the first two variability components can be explained through sampling of different radii in a smoothly stratified flow, the third component is radically different, with seed photons as well as electrons being very energetic. As it is tied to the highest frequencies, it likely originates in the innermost part of the flow. The spectral shape then points to this region being shielded from the soft seed photons from the disc by the softer Comptonization regions. Hence it should also have no reflection, as observed, although the uncertainties are large.

A further clue to the radial spectral stratification comes from subtracting the different frequency resolved spectra. Assuming the propagation framework is generally correct, these should mirror spectral components representative of the region where the variability component arises. While we are not able to directly fit any specific emission component to these spectra, the data by themselves indicate that L_2 arises in a higher energy environment than L_1. Both components resemble Comptonized emission rather than a blackbody, pointing to an optically thin flow rather than the accretion disc itself, consistent with a truncated disc geometry.

We can now put all our results in the context of the accretion geometry. The similarity of the subtracted spectra to Comptonization leads us to place the origin of the variability components in the hot inner flow. L_1 has both lowest frequency and the softest spectrum, and is thereby likely to arise furthest out in the flow. The spectrum of L_2 is slightly harder, placing it at smaller radii. However, both

these variability spectra show clear signs of reflection (such as a noticeable iron line), indicating that they cannot arise too far away from the thin, optically thick disc. In contrast, L_3 has a very hard spectrum which shows no sign of reflection, placing its origin well inside the disc truncation radius and close to the innermost regions of the flow. The seed photon temperature of several keV also makes it likely that they come from Comptonization in the outer parts of the hot flow, rather than directly from the disc. Combining emission from all these regions gives the total spectrum.

The general picture above assumes that the innermost regions (where the variability is most rapid) are also where the high-energy emission arises. In principle, this does not need to be the case. However, placing the high-energy emission further out in the flow creates a number of extra issues which must be resolved. First of all, the energy budget is highest in the innermost regions, making this the most likely region to produce the most energetic radiation. Secondly, the observed time lags (where hard emission lags the soft), are best explained by propagation from outer (soft) to inner (hard) regions of the flow (Kotov et al. 2001). Even more compelling is the spectral-timing information. Variations faster than the local viscous time-scale will be damped, and rapid variability will thus only arise in the innermost regions (within $\sim 10\, r_g$; see, e.g. Done et al. 2007). The fact that the rapid variability is proportionately strongest in the high-energy band, and that high energies dominate the spectra at high frequencies, strongly suggest that also the high-energy emission arises in the innermost region.

Even if we can paint a generally consistent picture, there are still questions which remain unanswered. For instance, a mechanism must be found to explain the frequencies of the variability components. If variability is created at all frequencies, why are these ones picked out? The most obvious answer is that the variability components are tied to certain radii in the flow, yet this does not match the fundamental assumption in propagation model, where fluctuations generated at one radii will propagate and thereby be present at all smaller radii. To prevent this, a mechanism must be invoked to allow one region to dominate, for example, by assuming increased emissivity at certain radii (perhaps as a response to increased turbulence) or causing fluctuations to dampen as they propagate. However, our current results alone do not allow us to test any such hypotheses, or to estimate values of these radii. For this, the analysis presented here needs to be combined with assumptions about the propagation speed, i.e. the viscous frequency in the hot flow. This is done in Mahmoud & Done (2018a).

While the results reported here constitute an important step in breaking the spectral degeneracy, it is clear that there are many issues left to solve, both in the propagating fluctuations framework and to understand these data. For example, while Rapisarda, Ingram & van der Klis (2017b) were able to find good agreement between model and observations for power spectra, time lags, and coherence as a function of energy in Cyg X-1 using propagating fluctuations, the same analysis showed discrepancies when applied to the BHB XTE J1550 − 564 (Rapisarda, Ingram & van der Klis 2017a). It is thus not surprising that also our results require the model to be refined in order to explain all observed features; indeed, such efforts are already underway (Mahmoud & Done 2018b). Equally important are more observational results, allowing us to look for systematic changes, for example, as a function of spectral state. Such analysis is in progress, and will be reported in a future paper (Axelsson et al. in preparation).

5 SUMMARY AND CONCLUSIONS

We have analysed the broad-band variability of Cyg X-1 in the low/hard state using frequency-resolved spectroscopy. We find that the two main power spectral components, L_1 and L_2, have spectra which are too soft to match the total spectrum at higher energies. A third variability component appears at higher frequencies in the power spectrum, and this component has a drastically harder spectrum. This is mainly due to its seed photon energy being substantially higher than those seen by the flow at larger radii. These results can be interpreted in terms of propagating fluctuations through a Comptonization cloud which is radially stratified. The outer regions see the seed photons from the disc, and Compton cool on them, producing soft spectra. These regions also shield the inner parts of the flow from direct illumination by the disc as they are (moderately) optically thick. We model this directly using only two Comptonization components, but subtraction of the spectral components indicates that there may be more gradual radial stratification of the outer region. This shows the potential of better data to directly deconvolve the radial properties of the hot inner flow, and hence determine whether this contains the imprint of the radius from which the compact jet is launched and powered.

ACKNOWLEDGEMENTS

This work was supported by The Carl Trygger Foundation (grant CTS 16:41) and Ivar Bendixsons foundation, and has made use of data obtained through the High Energy Astrophysics Science Archive Research Center (HEASARC) Online Service, provided by NASA/Goddard Space Flight Center. CD acknowledges STFC funding under grant ST/L00075X/1 and a JSPS long term fellowship L16581.

REFERENCES

Arévalo P., Uttley P., 2006, MNRAS, 367, 801
Axelsson M., Borgonovo L., Larsson S., 2005, A&A, 438, 999
Axelsson M., Borgonovo L., Larsson S., 2006, A&A, 452, 975
Axelsson M., Hjalmarsdotter L., Borgonovo L., Larsson S., 2008, A&A, 490, 253
Axelsson M., Hjalmarsdotter L., Done C., 2013, MNRAS, 431, 1987
Axelsson M., Done C., 2016, MNRAS, 458, 1778
Basak R., Zdziarski A. A., Parker M., Islam N., 2017, MNRAS, 472, 4220
Belloni T., Hasinger G., 1990, A&A, 227, L33
Belloni T., Psaltis D., van der Klis M., 2002, ApJ, 572, 392
Di Salvo T., Done C., Życki P. T., Burderi L., Robba N. R., 2001, ApJ, 547, 1024
Done C., Gierliński M., Kubota A., 2007, A&ARv, 15, 1
Fabian A. C., Ballantyne D. R., Merloni A., Vaughan S., Iwasawa K., Boller T., 2002, MNRAS, 331, L35
Fabian A. C., Parker M. L., Wilkins D. R., Miller J. M., Kara E., Reynolds C. S., Dauser T., 2014, MNRAS, 439, 2307
García J., Dauser T., Reynolds C. S., Kallman T. R., McClintock J. E., Wilms J., Eikmann W., 2013, ApJ, 768, 146
Gierliński M., Zdziarski A. A., Poutanen J., Coppi P. S., Ebisawa K., Johnson W. N, 1999, MNRAS, 309, 496
Grinberg V. et al., 2014, A&A, 565, A1
Hjalmarsdotter L., Axelsson M., Done C., 2016, MNRAS, 456, 4354
Ibragimov A., Poutanen J., Gilfanov M., Zdziarski A. A., Shrader C. R., 2005, MNRAS, 362, 1435
Jahoda K., Swank J. H., Giles A. B., Stark M. J., Strohmayer T., Zhang W., Morgan E. H., 1996, in Oswald H. S., Mark A. G., eds, Proc. SPIE Conf. Ser. Vol. 2808, In-orbit performance and calibration of the Rossi X-ray Timing Explorer (RXTE) Proportional Counter Array (PCA). SPIE, Bellingham, p. 59

Kolehmainen M., Done C., Díaz Trigo M., 2011, MNRAS, 416, 311
Kotov O., Churazov E., Gilfanov M., 2001, MNRAS, 327, 799
Laor A., 1991, ApJ, 376, 90
Leahy D. A., Darbro W., Elsner R. F., Weisskopf M. C., Sutherland P. G., Kahn S., Grindlay J. E., 1983, ApJ, 266, 160
Lyubarskii Y. E., 1997, MNRAS, 292, 679
Mahmoud R. D., Done C., 2018a, MNRAS, 473, 2084
Mahmoud R. D., Done C., 2018b, preprint (arXiv:1803.04811)
Makishima K. et al., 2008, PASJ, 60, 585
Markoff S., Nowak M. A., Wilms J., 2005, ApJ, 635, 1203
Miškovičová I. et al., 2016, A&A, 590, A114
Misra R. et al., 2017, ApJ, 835, 195
Miyamoto S., Kimura K., Kitamoto S., Dotani T., Ebisawa K., 1991, ApJ, 383, 784
Nowak M. A., 2000, MNRAS, 318, 361
Nowak M. A. et al., 2011, ApJ, 728, 13
Pottschmidt K. et al., 2003, A&A, 407, 1039
Poutanen J., Coppi P. S., 1998, Physica Scripta Volume T, 77, 57
Rapisarda S., Ingram A., van der Klis M., 2017a, MNRAS, 469, 2011
Rapisarda S., Ingram A., van der Klis M., 2017b, MNRAS, 472, 3821
Reig P., Papadakis I., Kylafis N. D., 2002, A&A, 383, 202
Revnivtsev M., Gilfanov M., Churazov E., 1999, A&A, 347, L23
Revnivtsev M., Gilfanov M., Churazov E., 2000, A&A, 363, 1013
Revnivstev M., Gilfanov M., Churazov E., 2001, A&A, 380, 520
Revnivtsev M. G., Gilfanov M. R., 2006, A&A, 453, 253
Wilms J., Allen A., McCray R., 2000, ApJ, 542, 914
Yamada S., Makishima K., Done C., Torii S., Noda H., Sakurai S., 2013, PASJ, 65, 80
Zdziarski A. A., Johnson W. N., Magdziarz P., 1996, MNRAS, 283, 193
Zdziarski A. A., Poutanen J., Paciesas W. S., Wen L., 2002, ApJ, 578, 357
Zhang W., Jahoda K., Swank J. H., Morgan E. H., Giles A. B., 1995, ApJ, 449, 930
Życki P. T., Done C., Smith D. A., 1999, MNRAS, 309, 561

This paper has been typeset from a TEX/LATEX file prepared by the author.